

Improvement of Fe/MgO Catalysts by Calcination for the Growth of Single- and Double-Walled Carbon Nanotubes

Guoqing Ning, Fei Wei,* Qian Wen, Guohua Luo, Yao Wang, and Yong Jin

Beijing Key Laboratory of Green Reaction Engineering and Technology, Department of Chemical Engineering, Tsinghua University, Beijing 100084, China

Received: September 22, 2005; In Final Form: November 14, 2005

Calcination at 900–1000 °C for 8–12 h of an Fe/MgO catalyst prepared by impregnation was found to result in a uniform $\text{MgFe}_2\text{O}_4/\text{MgO}$ solid solution that showed a successful settling of well-dispersed iron species into the MgO lattice. During methane reduction, many iron-containing particles with a diameter of about 4 nm were formed on the catalyst surface to provide numerous active sites for the growth of single- and double-walled carbon nanotubes. There was a significant improvement of the Fe/MgO catalyst that resulted in a high yield of impurity-free nanotubes. Using C_2H_4 cracking at 600 °C and transmission electron microscope observations, the Fe species distribution in the catalysts and microscope images of nanotube growth were described in detail. H_2 reduction of the calcined Fe/MgO catalyst was found to cause the formation of iron layers on the catalyst surface, which resulted in the growth of only carbon layers. The results are useful for understanding changes in the metal species distribution in the catalysts and the nanotube growth mechanism, and they provide a simple method to improve Fe/MgO catalysts.

Introduction

Since their discovery, carbon nanotubes (CNTs)^{1,2} have attracted much attention due to their unique structural, mechanical, and electrical properties.³ MgO-supported catalysts have been demonstrated to be efficient for single- and double-walled carbon nanotube (SWNT and DWNT) synthesis,^{4–6} and MgO can be removed by a relatively mild acid treatment. However, the carbon materials prepared by MgO-supported catalysts often contained carbon impurities, such as carbon nanofibers (CNFs), that cannot be removed by an acid wash. These impurities were found to be caused by the existence of poorly dispersed metal oxide species, such as Fe^{3+} clusters and MgFe_2O_4 -like particles in the Fe/MgO catalysts.⁷

As compared to the CoO–MgO and NiO–MgO solid solutions, FeO–MgO contains more defects,⁸ which is not favorable for the high dispersion of Fe species. Many efforts have been made to obtain MgO-supported catalysts with well-dispersed iron species, e.g. by varying the urea/nitrate ratio in a combustion method⁷ or using size-controlled iron oxide particles.⁹ However, the precise distribution of the metal species in the MgO-based powders was not clearly described, and the introduction of another reagent in the catalyst preparation may cause an undesirable influence in the growth of the nanotubes.

In this work, a uniform $\text{MgFe}_2\text{O}_4/\text{MgO}$ solid solution that did not show any evident residual iron oxide particles on the catalyst surface was obtained by a simple calcination. This showed a successful settling and the high dispersion of the iron species. It was found that the formation of metal particles and nanotubes occurred at nearly the same time during CH_4 reduction, which gave a microscopic picture of SWNT growth from a solid solution. This finding is meaningful for understanding the SWNT growth mechanism and improving the catalyst preparation technique.

Experimental Section

The Fe/MgO catalyst was prepared by impregnating MgO with an iron nitrate aqueous solution.¹⁰ The MgO carrier was prepared by heating alkaline magnesium carbonate at 500 °C. After ultrasonating the MgO powder in an iron nitrate aqueous solution, the resulting gel was dried at 120 °C and then ground to a fine powder. Finally the powder was calcined at 650 °C. The loading capacity of $\text{Fe}(\text{NO}_3)_3 \cdot 9\text{H}_2\text{O}$ was 0.014 mol/mol MgO.

In a typical experiment, the calcination of the Fe/MgO catalyst was conducted in air at 950 °C for 10 h. Carbon nanotube growth was performed at 900 °C by introducing a mixture of 95% methane and 5% H_2 for 20 min to the noncalcined or the calcined Fe/MgO catalyst placed in a vertical quartz tube.

The catalysts and the as-prepared carbon materials were characterized by transmission electron microscope (TEM, JEM-2010), scanning electron microscope (SEM, JSM-7401F), and BET specific surface area (SSA) measurement.¹¹ Raman spectrum (Renishaw, RM2000) and TGA (TGA-2050) were used to describe the purity and quality of the SWNTs and DWNTs. X-ray diffraction (XRD, D8 Advance) and X-ray photoelectron spectroscopy (XPS, PHI-5300) were applied to obtain information of substance structure and surface element composition of the catalysts.

Results and Discussion

Growth of SWNTs and DWNTs. In the nanotube materials prepared using the noncalcined catalyst, SWNTs were the main product, with some carbon nanofibers, which were due to the existence of large iron species particles on the catalyst⁷ being sporadically found. The TG curve (Figure 1a) showed the yields of amorphous carbon, SWNTs, and CNFs as 5.9 wt %, 3.0 wt %, and 0.4 wt %, respectively. However, when CH_4 cracking was performed over the calcined catalyst, an impurity-free product with a high nanotube yield was obtained. Parts a and b

* To whom correspondence may be addressed. Fax: +86-10-62772051. E-mail: weifei@flotu.org.

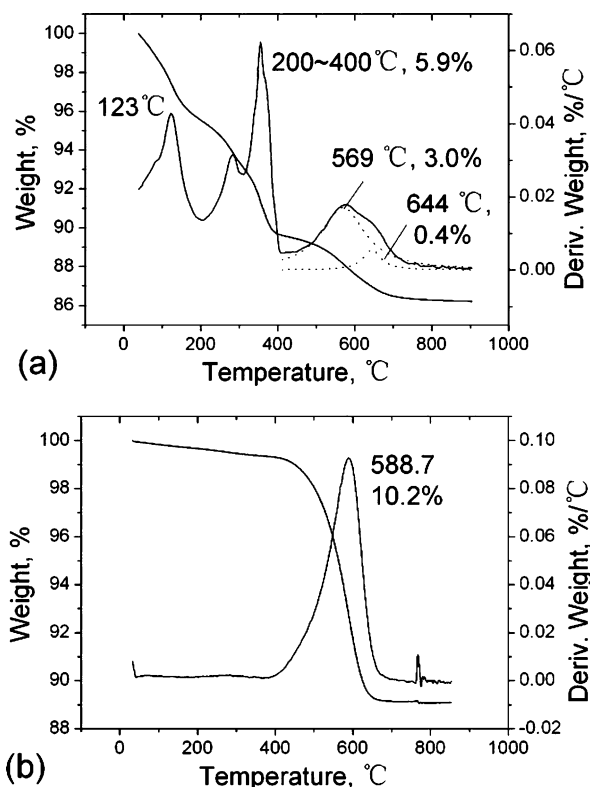


Figure 1. TGA curves of the as-prepared carbon material from the noncalcined Fe/MgO catalyst (a) and the catalyst calcined at 950 °C for 10 h (b). The conditions of TGA are 10 °C/min ramp rates at an air flow rate of 100 sccm.

of Figure 2 show that the product contains plentiful SWNTs and DWNTs, and no carbon impurities were found in a large number of SEM observations. TEM observation (Figure 2c) showed that the as-prepared nanotube material contains a mixture (A) of SWNTs (B) and DWNTs (C) with diameters from 1 to 5 nm. The TG curve (Figure 1b) showed a single peak at 588.7 °C, which corresponded to 10.2 wt % SWNTs and DWNTs. Taking into consideration the low iron content (0.014 mol/ mol MgO), the nanotube yield of 10.2 wt % is a better result than the reported yield of not more than 6 wt % obtained by similar Fe/MgO catalysts in the literature.^{12,13} This result was easily reproducible, and the calcination was confirmed as the key factor for the enhancement in SWNT growth.

Mechanism for the Improvement of Fe/MgO Catalyst for Nanotube Growth. By a comparative investigation of the noncalcined and the calcined catalysts, the morphology of the catalysts and the distribution of iron species was found to be markedly changed by the calcination. For the noncalcined Fe/MgO catalyst, the BET specific surface area (SSA) was 43.3 m²/g, and most of the particles had diameters of about 20–30 nm (Figure 3a). However, for the calcined catalyst, the BET SSA decreased to 8.1 m²/g, and the particle diameters increased to more than 100 nm (Figure 3b), which suggested that particle agglomeration had occurred. In the TEM observation shown in Figure 3a, there were some clear iron species particles that showed a dark contrast and also iron-free MgO particles that showed a light contrast.¹⁴ Such an agglomeration of iron species in Fe/MgO catalysts has been also reported by Ago et al.¹⁴ However, for the calcined catalyst, no iron particle was found in many TEM observations. The electron beam diffraction patterns (Figure 3 inset) show that the noncalcined catalyst was composed of polycrystals, in contrast with the mainly single crystals seen with the calcined catalyst. X-ray photoelectron spectroscopy (XPS) analysis showed the surface Fe to Mg

atomic ratio (with depth of ~3 nm) of the noncalcined and the calcined catalyst were 0.019 and 0.14, respectively. The surface Fe to Mg atomic ratio of the calcined catalyst was much higher than the total Fe content of 0.014, which indicated that there was Fe species enrichment on the catalyst surface due to the calcination. Together with the XRD analysis (Figure 4), it can be suggested that the iron species in the calcined catalyst are in the form of the Fe₂MgO₄ structure as a diluted dispersion in the MgO lattice. It is probable that such a well-dispersed iron in a MgFe₂O₄/MgO solid solution was formed by the interdiffusion between FeO_x and MgO.^{14,15}

Furthermore, experiments using C₂H₄ cracking at 600 °C over the noncalcined and the calcined catalysts showed that the iron species in the calcined catalyst were fully dispersed in the MgO lattice and no iron oxide particles remained on the MgO surface. It is well-known that ethylene is cracked at 600 °C by catalytic decomposition. As shown in Figure 5a, the carbon material prepared by C₂H₄ cracking over the noncalcined Fe/MgO catalyst contained many carbon nanofibers and multiwall carbon nanotubes. However, the material prepared over the calcined catalyst is gray in color and contained neither carbon fiber nor nanotube as shown in Figure 5b, which indicated that ethylene cracking did not occur. Taking into consideration that the iron oxide particles on the noncalcined catalyst had been reduced and became active sites for carbon deposition, this result indicated that there were no iron oxide particles on the calcined catalyst and the temperature of 600 °C was not high enough to activate the stable MgFe₂O₄/MgO solid solution. These results suggested that the iron species in the calcined catalyst have been fully dispersed in the MgO lattice and no clusters of iron species remained on the MgO surface. The results also imply that the active catalytic species for the growth of CNTs is the metal rather than the oxide solid solution.¹⁶

A formation mechanism of the MgFe₂O₄/MgO solid solution is proposed in Figure 7a–c. There are three factors in favor of a high dispersion of the iron species: (i) the support material is porous and easily agglomerates, which allows the iron species to contact MgO over a large surface area; (ii) the strong interaction between iron oxide and MgO prevents iron particle agglomeration during the heat treatment;¹⁴ (iii) the content of iron is low at 0.014 mol per mol MgO, which makes it easy for all the iron to diffuse into the MgO lattice without any iron particle remaining, although the solid diffusion rate is quite limited.

To understand the SWNT growth mechanism over the calcined catalyst, a carbon deposition of only 0.5 min was conducted. As shown in Figure 6a, in the as-prepared carbon material, many small dark dots with a diameter within a small range of 3.5–4.2 nm were found evenly dispersed on the catalyst surface, which had shown a uniform appearance before the methane cracking (Figure 3b). It is probable that these dark dots are iron-enriched particles that formed by the precipitation of iron species¹⁴ from the MgFe₂O₄/MgO solid solution due to the reduction by methane. These iron-enriched particles should also contain carbon deposits from methane cracking. In Figure 6b, it is shown that in addition to graphite layers around the iron-enriched particles (A), there were also SWNTs growing from them (B, C, and D). This indicates that these iron-enriched particles were newly formed active sites for SWNT and DWNT growth. In careful observations, it can be found that most of the iron-enriched particles appear at the ends of different MgO planes. This suggests that the direction of iron diffusion in the MgO lattice is parallel to the MgO planes, and iron diffusion between different MgO planes can be ignored. This is important

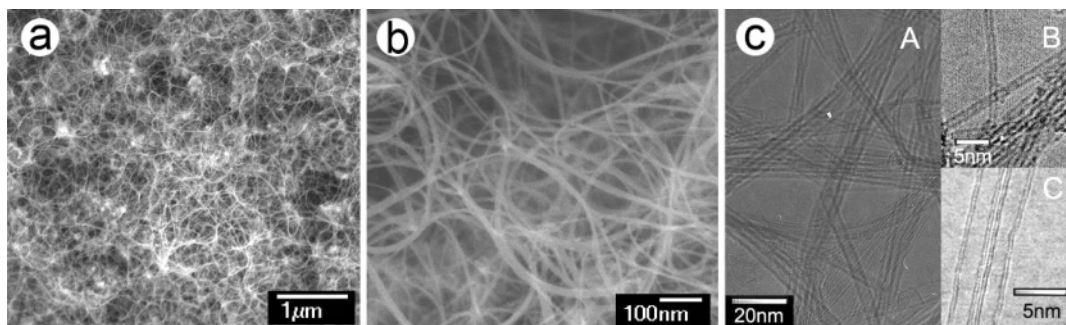


Figure 2. SEM (a, b) and TEM (c) images of the nanotube material prepared by methane cracking over the Fe/MgO catalyst calcined at 950 °C for 10 h.

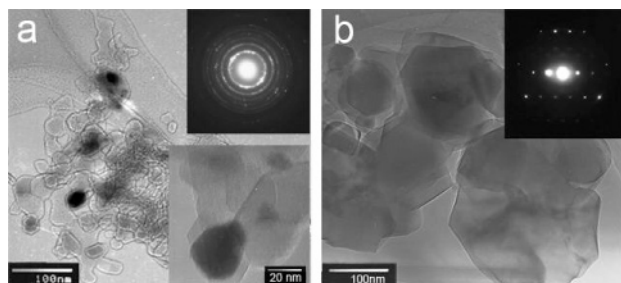


Figure 3. TEM images and electron beam diffraction patterns (as inset) of the noncalcined Fe/MgO catalyst (a) and the catalyst calcined at 950 °C for 10 h (b).

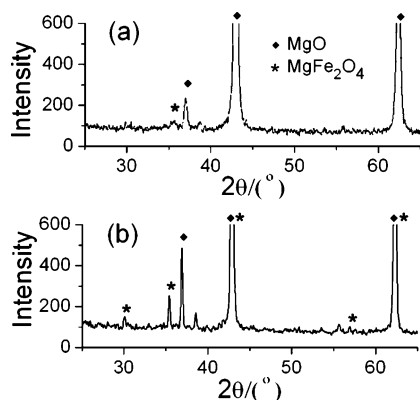


Figure 4. XRD spectra of the noncalcined (a) and the calcined Fe/MgO catalyst (b).

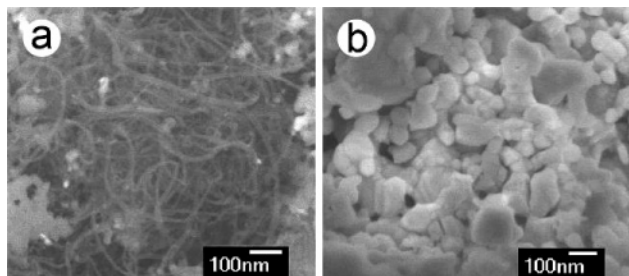
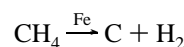


Figure 5. SEM images of the materials prepared by C₂H₄ cracking at 600 °C over the noncalcined (a) and calcined Fe/MgO catalyst (b).

for avoiding agglomeration of the newly formed metal particles. Figure 6c suggests that both the tip growth¹⁷ (E, F) and the base growth¹⁸ modes (G) occur in the growth of nanotubes with diameters of about 5 nm.

The proposed mechanism of calcination and nanotube growth is shown in Figure 7. Calcination causes FeO_x clusters to be well-dispersed in the MgO lattice, resulting in the MgFe₂O₄/MgO solid solution. After the introduction of methane, many small iron-enriched particles with diameters less than 5 nm

appear on the catalyst surface. This results in many more active sites for nanotube growth when compared with the noncalcined catalyst. This may be the reason calcination has significantly promoted the growth of SWNTs and DWNTs. The reactions of iron species reduction and carbon deposition can be described as follows:



Carbon from methane cracking can be dissolved in these iron-enriched particles, which leads to the formation of carbon nanotubes at the same time as the formation of the particles. This is an important factor that prevents the iron-enriched particle from growing larger. The diffusion rate of the iron species in the solid is slow, which also works to avoid the iron particles from growing larger.

Calcination Temperature and Time Dependence. The temperature range 900–1000 °C was found to be appropriate for improving the catalyst performance (see Figure S-1, Supporting Information). A calcination temperature of 850 °C was too low for the iron species to be well-dispersed. A calcination temperature of 1100 °C would lead to a compact surface of MgO, which is not conducive for gas diffusion and will depress nanotube growth.

Concerning the calcination time, a time of 8–12 h is appropriate (see Figure S-2, Supporting Information). A short time calcination, such as 4 or 6 h, was not enough to improve the noncalcined catalyst even at an appropriate temperature. A long time calcination in Ar, such as 16 or 48 h, will cause the iron species to sinter, leading to the growth of carbon nanofibers. This result is consistent with the XPS analysis of the calcined catalyst, which showed an enrichment of the iron species on the catalyst surface. Calcination in air can prevent such sintering of the Fe species even when carried out for 24 h. The reason for the different changes in the iron species when the calcination is in Ar or in air is still not clear. It may be that the sintering of the iron species is due to the decomposition of FeO_x when the calcination is performed under Ar for a long time, but this does not occur in air due to the existence of oxygen.

Influence of MgO Morphology. The formation of the uniform MgFe₂O₄/MgO solid solution was found to be related to the crystallinity and porosity of the MgO carrier. Since the iron content was quite small, the agglomeration behavior of the Fe/MgO catalysts can be characterized by that of MgO. Two kinds of MgO were used for comparison: one was prepared by calcining MgCO₃ at 500 °C, labeled MgO-A; the other is a chemical reagent used as purchased, labeled MgO-B. The BET SSAs of MgO-A and MgO-B are 78.2 m²/g and 27.4 m²/g, respectively. TEM observations (see Figure S-3, Supporting

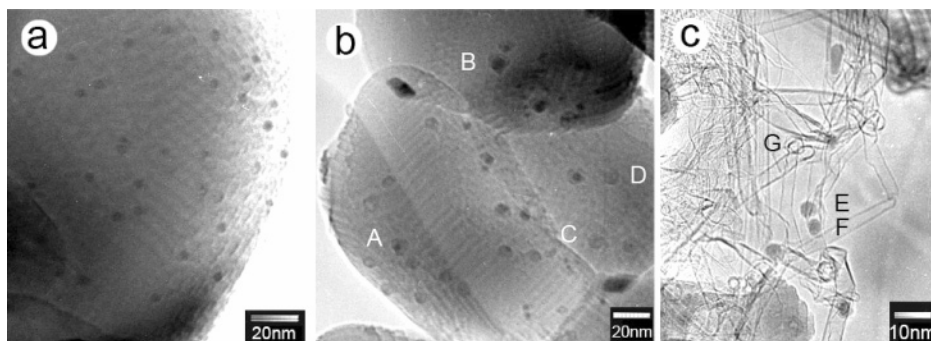


Figure 6. TEM images of the material prepared by methane cracking at 900 °C for 0.5 min over the calcined Fe/MgO catalyst.

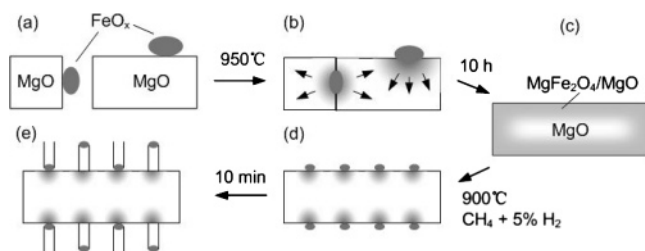


Figure 7. Proposed mechanism of the heat treatment and SWNT growth over the Fe/MgO catalyst: (a) the noncalcined Fe/MgO catalyst prepared by impregnation; (b, c) formation of the $\text{MgFe}_2\text{O}_4/\text{MgO}$ solid solution by heat treatment at 950 °C for 10 h from the diffusion of iron into the MgO lattice; (d) some small iron-enriched particles appearing on the surface of the catalyst particle due to reduction by the CH_4 reactant at 900 °C; (e) carbon nanotube growth from the iron-enriched particles.

Information) showed that MgO-A contained many small particles with diameters of 10–20 nm, and the largest particles are less than 50 nm. The fringes of the particles are irregular, forming a porous structure, which can be attributed to CO_2 release during MgCO_3 decomposition. As compared to MgO-A, MgO-B contains much larger particles with diameters of 100–200 nm, and the particles are of good crystallinity with a regular shape. When calcination at 950 °C for 10 h was performed, MgO-A agglomerated much easier than MgO-B due to the high SSA and the porous structure. The BET SSAs of heat-treated MgO-A and MgO-B are 12.7 m^2/g and 11.8 m^2/g , respectively, as compared to 8.09 m^2/g for the heat-treated Fe/MgO-A catalyst, suggesting that the existence of iron species can promote particle agglomeration during the calcination.

In the case when MgO-B was used as the support, calcination at 950 °C for 10 h did not improve the Fe/MgO-B catalyst visibly, and many nanofibers were still found in the as-prepared carbon material. This indicates that the crystallinity and porosity of the MgO carrier are key factors affecting the dispersion of the iron species during calcination. This is consistent with the mechanism shown in Figure 7. All the Fe/MgO catalysts used in this work were prepared using MgO-A as the support except for those specified otherwise.

Influence of Hydrogen Reduction. The calcined catalyst was found to be sensitive to hydrogen reduction. In this experiment, after hydrogen reduction at 900 °C for 20 min, carbon deposition was performed by introducing a reactant flow to the calcined catalyst for 10 min. The Raman spectrum is depicted in Figure 8b. The hydrogen-reduced catalyst shows a much stronger D-band signal compared with the sample without a hydrogen reduction (Figure 8a). This indicates that much carbon impurities were formed due to the hydrogen reduction treatment. SEM and TEM observations showed that the formation of SWNTs and DWNTs was suppressed strongly by prior hydrogen reduction,¹⁴ and the main form of carbon deposited was amorphous carbon

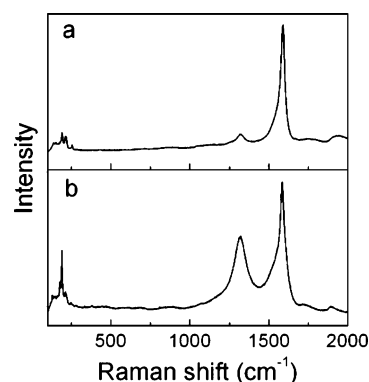


Figure 8. Raman spectra of the carbon materials prepared over the calcined Fe/MgO catalysts without hydrogen reduction (a) and with hydrogen reduction for 20 min (b).

layers covering the catalyst surface (Figure 9a and b). TGA showed that the carbon content in the as-prepared material was 6.8 wt %. Liu et al.¹⁹ reported that the hydrogen reduction of an Fe/MgO catalyst gave a different effect in comparison with methane reduction: the XRD pattern of the hydrogen-reduced Fe/MgO catalyst showed an obvious iron peak, as compared to an almost inconspicuous iron peak from the methane-reduced catalyst (Figure 10). The TEM image of the catalyst obtained after 20 min hydrogen reduction of the calcined Fe/MgO catalyst (Figure 9c) showed iron species gathering on the surface of the catalyst particles, since the dark area on the particle surface has an irregular shape that cannot be caused by overlap or a large thickness of MgO. These results suggest that the well-dispersed iron species in the calcined catalyst had been reduced to metallic iron, which separates out and gathers as iron layers on the particle surface. When a carbon-depositing reactant gas was introduced to the hydrogen-reduced catalyst, carbon layers formed on the surface of the iron layers due to a rapid carbon deposition caused by the high activation of these iron layers. Since there is a large contact area, the carbon layers combine tightly with the catalyst particles, resulting in a parallel growth of new carbon deposits. When the carbon layers have covered the surface of the iron layers, methane diffusion into the iron layers is blocked, which leads to catalyst deactivation. The phenomenon of iron precipitation caused by hydrogen reduction also provides further evidence for the formation mechanism of the iron-enriched particles shown in Figure 7.

Conclusion

A simple method to disperse iron species into MgO lattices that does not leave any iron oxide particles on the MgO surface was presented. A heat treatment at 900–1000 °C for 8–12 h was found to significantly improve an Fe/MgO catalyst for SWNT growth that gave much better purity and yield. The

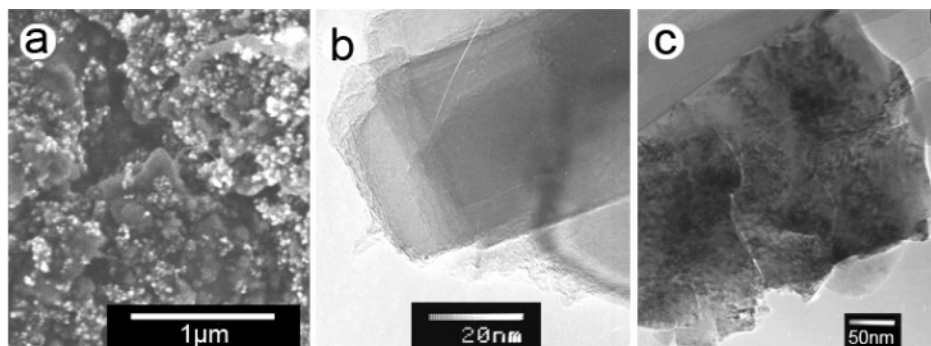


Figure 9. SEM (a) and HRTEM (b) images of the carbon material prepared with prior hydrogen reduction of the calcined Fe/MgO catalyst, and the TEM image (c) of the catalyst obtained by 20 min hydrogen reduction of the calcined Fe/MgO catalyst.

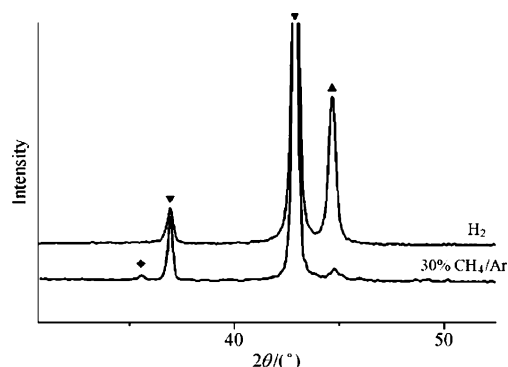


Figure 10. XRD spectra of Fe/MgO catalysts (Fe:Mg = 1:10) reduced by hydrogen or methane at 1000 °C: (▲) Fe, (▼) MgO, (◆) MgFe_2O_4 .¹⁹

mechanism of this improvement by the heat treatment was the diffusion of the iron species during the calcination that led to a high dispersion of the iron species in the MgO lattice, resulting in a uniform $\text{MgFe}_2\text{O}_4/\text{MgO}$ solid solution. When methane was exposed to the heat-treated catalyst at 900 °C, many small iron-enriched particles (<5 nm) appear on the catalyst surface due to the reduction by methane. These are active sites for SWNT growth.

Hydrogen reduction for 20 min will cause the formation of large iron layers on the support surface. When methane was exposed to the reduced catalyst, carbon layers covering the catalyst particles are formed, which significantly depresses SWNT growth.

Acknowledgment. We thank Prof. Dezheng Wang for touching up of this paper. This work is supported by the Chinese National Natural Science Foundation under contract number 20236020.

Supporting Information Available: SEM images of the as-prepared carbon materials using Fe/MgO catalysts calcined at different temperatures for 10 h (Figure S-1), SEM images of

the as-prepared carbon materials using Fe/MgO catalysts calcined at 900 °C for different times (Figure S-2), and TEM images of MgO-A, MgO-B, and powders prepared by calcining MgO-A or MgO-B at 950 °C for 10 h (Figure S-3) (PDF). This material is available free of charge via the Internet at <http://pubs.acs.org>.

References and Notes

- (1) Iijima, S. *Nature* **1991**, 354, 56.
- (2) Iijima, S.; Ichihashi, T. *Nature* **1993**, 363, 603.
- (3) Dresselhaus, M. S.; Dresselhaus, G.; Avouris, P. *Carbon Nanotubes Synthesis, Structure, Properties, and Applications*; Springer: New York, 2001.
- (4) Li, Q. W.; Hao, Y.; Li, X. H.; Zhang, J.; Liu, Z. F. *Chem. Mater.* **2002**, 14, 4262.
- (5) Flahaut, E.; Bacsá, R.; Peigney, A.; Laurent, C. *Chem. Commun.* **2003**, 1442.
- (6) Flahaut, E.; Peigney, A.; Laurent, C.; Rousset, A. *J. Mater. Chem.* **2000**, 10, 249.
- (7) Coquay, P.; Peigney, A.; Grave, E. D.; Vandenberghe, R. E.; Laurent, C. *J. Phys. Chem. B* **2002**, 106, 13199.
- (8) Hu, Y. H.; Ruckenstein, E. *Catal. Rev.* **2002**, 44, 423.
- (9) Ago, H.; Nakamura, K.; Imamura, S.; Tsuji, M. *Chem. Phys. Lett.* **2004**, 391, 308.
- (10) Li, Q. W.; Yan, H.; Cheng, Y.; Zhang, J.; Liu, Z. F. *J. Mater. Chem.* **2002**, 12, 1179.
- (11) Ning, G.; Wei, F.; Luo, G.; Jin, Y. *Carbon* **2005**, 43, 1439.
- (12) Flahaut, E.; Govindaraj, A.; Peigney, A.; Laurent, C.; Rousset, A.; Rao, C. N. R. *Chem. Phys. Lett.* **1999**, 300, 236.
- (13) Colomer, J. F.; Stephan, C.; Lefrant, S.; Van Tendeloo, G.; Willems, I.; Konya, Z.; Fonseca, A.; Laurent, C.; Nagy, J. B. *Chem. Phys. Lett.* **2000**, 317, 83.
- (14) Ago, H.; Nakamura, K.; Uehara, N.; Tsuji, M. *J. Phys. Chem. B* **2004**, 108, 18908.
- (15) Gao, Y.; Kim, Y. J.; Thevuthasan, S.; Chambers, S. A.; Lubitz, P. *J. Appl. Phys.* **1997**, 81, 3253.
- (16) Tian, Y.; Hu, Z.; Yang, Y.; Wang, X.; Chen, X.; Xu, H.; Wu, Q.; Ji, W.; Chen, Y. *J. Am. Chem. Soc.* **2004**, 126, 1180.
- (17) Huang, S. M.; Woodson, M.; Smalley, R.; Liu, J. *Nano Lett.* **2004**, 4, 1025.
- (18) Zhang, Y.; Li, Y.; Kim, W.; Wang, D.; Dai, H. *Appl. Phys. A* **2002**, 74, 325.
- (19) Liu, J. X.; Ren, Z.; Duan, L. Y.; Xie, Y. C. *Acta Chim. Sin.* **2004**, 62, 775.